LA-UR- 99-5838

Title: Analysis of shock damage to Berea sandstone using SEM images of samples from impact recovery experiments

Author(s): C. R. Hagelberg, M. Hiltl, R. P. Swift, and W. J. Nellis

Submitted to: ETCE/OMAE 2000 Joint Conference: Energy for the New Millenium. February 14-17, 2000, New Orleans, LA

and
Journal of Energy Resources Technology

Los Alamos
NATIONAL LABORATORY

Proceedings of the ETCE/OMAE 2000 Joint Conference:
Energy for the New Millenium
February 14-17, 2000, New Orleans, LA

PR-058

ANALYSIS OF SHOCK DAMAGE TO BEREA SANDSTONE USING SEM IMAGES OF SAMPLES FROM IMPACT RECOVERY EXPERIMENTS

Carl. R. Hagelberg[1] **Michael Hiltl**[2]
Robert P. Swift[1] **William J. Nellis**[2]

[1]Los Alamos National Laboratory

[2]Lawrence Livermore National Laboratory

ABSTRACT. A series of impact recovery experiments have been conducted on dry, water-saturated (wet), and water-pressurized Berea sandstone samples using a single stage light gas gun. The samples are subjected to various stress levels using a flyer plate impact. The recovered samples provide a large database of Scanning Electron Microscope (SEM) images depicting the damage. Laser particle size analyses are also being conducted on portions of the recovered samples to characterize changes in grain size distribution. We present the characteristics of the recovered samples using the SEM for selected examples from each of the experimental categories. We also present some preliminary statistical analysis of the SEM images of the samples to assess variations in damage.

INTRODUCTION. A series of shock recovery experiments have been performed on samples of Berea sandstone using a single stage light gas gun (Hiltl et al, 1999ab). Berea sandstone is commonly used as a standard in petrophysical studies. The porosity of Berea has been measured to be 21.9% and contains various minerals consisting of 75% quartz, 10% clay, 10% feldspar, and 5% calcite, with an average grain size of 0.15 mm (Zhang et al, 1990). The shock recovery experiments were designed to characterize the results of various shock loadings of sandstone under dry, water saturated, and water pressurized conditions. Presented here are general characteristics of the experimental results as well as preliminary results from applications of statistical analyses to SEM images of the recovered samples. The analyses are intended to distinguish the various experimental results through evaluation of the corresponding SEM images of the recovered samples. An intuitive notion of “damage” to the original grain structure is based largely on the human visual system. The statistical analyses are one means of quantifying the spatial variability in the SEM images and relating that to the saturation and stress conditions of the experiments. The experiments analyzed here are a necessary part of developing an understanding of the basic principles involved in the physics of well completion using shaped charges. During the process of completion the reservoir material is exposed to a shock produced by the shaped-charge jet. The shock produces damage to the rock and potentially reduces permeability due to the creation of fine particles that may clog flow paths (Harris, 1966; McLeod, 1983; and Haleck, 1996) . Here we are interested primarily in finding methods of distinguishing between levels of grain damage in a statistical sense so that we may provide a methodology for understanding the global results of shock loading. Applying similar techniques to the results of mesoscale simulations provides one method for model verification (Hagelberg et al, 1999; Swift et al, 2000). The analysis techniques will potentially lead to a means of upscaling experimental and modeling results to phenomenological models that describe the macro behavior of a well completion.

EXPERIMENTS. The experiments cover a range of impact stresses by using PMMA, aluminum, and copper flyer plates, and a range of saturation conditions (dry, wet, and water- pressurized). Impact stresses were selected in the range from 1.3 GPa to 9.8 GPa. Figure 1 shows a schematic diagram of the set-up for the water pressurized experiments. In the first set of experiments the samples were disk shaped of approximately 25 mm in diameter and 5 mm thick. We found that the stress wave did not attenuate in such a thin sample and chose to increase subsequent samples to 15 mm thickness while retaining the 25 mm diameter (restricted by the bore size of the gas gun). Attenuation of the stress wave is observable in some of the 15 mm samples. Table 1 specifies the conditions of the subset of experiments discussed here.

The reduction in damage is illustrated in Figure 2, where SEM images at 400x magnification close to (near field) and far from (far field) the impact surface are shown for dry, wet, and water pressurized conditions. The impact pressures are in the range 6.1 GPa to 6.4 GPa. While both locations show extensive grain fragmentation there is an observable difference between the two locations. The damage decreases away from the impact surface, and from dry to wet to water-pressurized conditions. Figure 3 shows six SEM images at 400x magnification of lower impact pressures (1.2 GPa to 1.4 GPa) on dry, wet, and water pressurized and the same qualitative results are observed. Further evidence of damage reduction with distance from impact is found by performing laser particle size analyses on subsample at various distances from the impact surface. Figure 4 shows the size distributions for an undamaged Berea sample and for two different locations within a single shock recovery experiment (#606, 6.1GPa dry). The reduction in damage away from the impact is observed in the relationships between the size distributions and lends support to the observations obtained through SEM imaging.

The heterogeneous nature of the damage can be seen in most of the images but particularly stands out in Figure 2E and Figure 3A. It is possible to find areas where there is little damage adjacent to areas with extensive fragmentation, especially for the experiments with lighter shock loadings and/or water in the pore space. The results emphasize that the shock wave damage is very dependent on the meso-scale structure of the boundaries of the grains and the interaction between grains.

SEM DATA. Samples were examined using a Noran Instruments, Incorported ADEM (Automated Digital Electron Microscope) SEM. Backscattered electron signals were used to generate digital images with either 512 by 512 or 1024 by 1024 pixel resulution. Images were acquired at both 100 and 400 X magnification. Column conditions were 20 kV accelerating potential. Nominal beam currents were 100 to 500 picoamperes. All samples were coated with approximately 200 angstroms of carbon prior to examination. Many references are available on SEM techniques (e.g. Goldstein et al, 1981).

An example of an SEM image (100 X) of undamaged Berea sandstone is shown in Figure 5. The vertical black lines are for reference in the subsequent text, and are spaced at 400μm intervals. The gray level is related to the average atomic number of the mineral. The larger the density of the material, the brighter it appears in the image. However, different minerals (for examples quartz, dolomite and sodium feldspar) can have similar average atomic numbers and will have similar gray levels. Such classes of minerals can be distinguished using x-ray analysis. The pores in the pictures appear dark, because they are filled with a low-density epoxy resin. So, generally, the pores are dark and the grains are light or middle gray, where we consider all minerals to be some type of 'grain'. The quartz grains (and all others) vary greatly in shape and boundary regularity. The heterogeneity of the material adds to the challenges of statistical analysis.

The "raw" images as they are provided by the SEM instrument can vary in contrast, gray scale range, local contrast, and pixel noise variance. Some of the variability is demonstrated in Figure 6, where the gray-scale histogram for three images are shown. The range in contrast and the location of highest frequency is somewhat different for each of the images. A key point is that each of the histograms has approximately the same shape, and therefore transforming the pixels of one image so that the histograms are the same will not affect the relative attributes in the image. In order to apply statistical techniques to compare multiple images we first modify each image through a histogram matching algorithm (Bidasaria, 1986) so that it matches a selected reference image. In the present context the reference image used was the raw image of undamaged Berea sandstone corresponding to Figure 5. Figure 7 shows the gray-scale histogram for three images: an undamaged Berea image (solid curve), an unprocessed post-shock image (wet 6.1 GPa, dotted), and the post histogram matched image (heavy dashed curve, coincident with the solid curve). After histogram matching the images may be compared using analyses that might otherwise be biased by a change in the SEM gain or contrast.

Figure 8 shows two examples of SEM images at 100x magnification that are used for the statistical analysis in the following section. Naturally, less detail is apparent when compared to the 400x images of Figures 2 and 3, however, at 100x there is a larger field of view that captures a larger and more consistent sample of the heterogeneity.

STATISTICAL ANALYSIS. We begin by examining transects of images to characterize various aspects of the spatial variability. Adjacent transects (columns of pixels) are correlated since they are passing through the same structures only a few microns apart. As the separation distance between transects increases the correlation decreases. The rate of decorrelation depends on the specific transect, but gives an idea of the general decorrelation length scales. Figure 9 shows the correlation coefficient between transects as a function of the transect spacing for two different locations. The correlation decreases from 1.0 to 0.0 within about 80 μm and then oscillates between +/-0.25. This suggests that the transects chosen at a spacing of 400μm (Figure 5) are well outside a typical spacing exhibiting correlation. To confirm this the correlation between each pair of transects was computed and all were less in magnitude than 0.223.

For each transect we apply a standard measure of spatial variance used in geostatistics. Namely, the sample semivariogram defined by

$$\hat{\gamma}(h) = \frac{1}{2N_h} \sum_{|\mathbf{s}_i - \mathbf{s}_j| = h}^{N_h} [Z(\mathbf{s}_i) - Z(\mathbf{s}_j)]^2 \qquad (1)$$

In equation (1), γ is the semivariance, $Z(s_k)$ is the gray-scale value of the image transect sample at location s_k , the position of the pixel measured from the bottom of the image. The lag distance, h, is the scalar distance $|s_i - s_j|$ since pixels lie along a specified transect, but more generally is a directional vector. The number of lag-h differences is N_h. Equation (1) represents (one-half of) the sample variance of the lagged differences in image intensity (Matheron, 1963; Journel and Huijbregts, 1978; Cressie, 1985; Isaaks and Srivastava, 1989; Deutsch and Journel, 1992). In the current application we are only concerned with two categories of pixels: grains and pores. Therefore, we apply a threshold to the images and compute the semivariance of the indicator images, i.e. the indicator semivariogram. Figure 10 shows the indicator semivariograms for the transects through the image of the undamaged Berea (Figure 5). Also shown in Figure 10 is the indicator semivariance of the entire image (dotted curve) where each column of the image is used as a transect and the difference set is taken over all transects simultaneously. Semivariograms are typically described in terms of the nugget effect, which is the value of the variogram at the first non-zero lag (Isaaks and Srivastava, 1989); the range, which is the lag spacing at which the semivariance asymptotically approaches a constant; and the sill, which is the value of the semivariance at the range. The nugget effect is a measure of the spatially independent noise variance, the range is a measure of the most significant transition frequency between grains and pores, and the sill minus the nugget is the spatially dependent structural variance. For the undamaged Berea, Figure 10 shows that any given transect has some oscillatory structure in the sill, while the entire image semivariance shows a nearly constant sill. The oscillatory structures in the transect semivariograms are due to the influence of the grains (note that the peak to trough length is approximately 140μm which corresponds to a frequency peak in the particle size analysis of Figure 4).

We apply the simple technique of finding the first zero crossing of the derivative of the semivariogram to locate the range. While the technique is expedient it must be noted that a preferred method would be to fit a variogram model to each graph, and use the resulting model parameters to identify the range. Using the derivative technique, the range for the undamaged Berea semivariogram based on the entire image (dashed line, Figure 9) is 106μm.

Figures 11 through Figures 16 show indicator semivariograms for each of the experiments shown in Figures 2 and 3, based on 100x SEM images of the near and far fields. Table 1 shows the resulting ranges for each of the full image semivariograms. For the higher impact pressure the results are intuitively consistent. The statistical length scales increase from dry to wet to water-pressurized. Also, the far-field length scales are larger than the near-field indicating a reduction in damage away from the impact. For the low pressure impact experiments (second set in Table 1, and Figures 14 through Figures 16) the range estimation results are not convincing.

DISCUSSION. We have shown how a classical statistical analysis of spatial continuity applies to SEM images from samples recovered from flyer plate impact experiments. A first set of technical difficulties is encountered due to the variation in gain and offset (contrast) in the SEM instrument itself and the translation of these drifts into the digital images used for statistical analyses. Compensation using histogram matching mitigates some of the differences. Still it is apparent that the indicator semivariograms are sensitive to the choice of the threshold value. Some results using the indicator semivariogram to estimate statistical length-scales using the range of the semivariogram appear useful for comparing various experimental conditions. Also, differences between individual transect semivariograms in the sill is apperent. A thorough frequency analysis of the sills may prove useful for identifying structure sizes within the various experimental results.

REFERENCES.

Bidasaria, H. B., 1986, “A method for almost exact histogram matching for two digitized images”, *Computer Vision, Graphics and Image Processing,* Vol. 34, pp. 93-98.

Deutsch, C. and A. Journel, 1992, *GSLIB Geostatistical Software Library and User’s Guide*, Oxford University Press, New York.

Goldstein, J. I., Newbury, D. E., Echlin, P., Joy, D. C., Fiori, C. and Lifshin, E., 1981, "Scanning Electron Microscopy and X-ray Microanalysis", Plenum Press, New York.

Hagelberg, C. R., R. P. Swift, T. C. Carney, D. Greening, M. Hiltl, and W. J. Nellis, 1999, “Modeling Shock Recovery Experiments of Sandstone”, in Shock Compression in Condensed Matter-1999 edited by M. D. Furnish, AIP Conference Proceedings (in press).

Halleck, P., 1996, “Studies Reveal Fractured Reservoir Perforating Damage”, *Pet. Eng. Int*., Vol. 69 (4), pp. 35-44.

Harris, M., 1966, “The Effect of Perforation on Well Productivity”, *J. Pet. Tech.,* pp. 518-28, Trans. of Am. Inst. Mining and Met. Eng. 237.

Hiltl, M., R. P. Swift, C .R.Hagelberg, T. C. Carney, and W. J. Nellis, 1999a, “ Shock-recovery experiments of sandstone under dry, wet, and water-pressurized conditions”, Proceedings, 11th topical conference on shock compression of condensed matter 1999, *Shock Compression in Condensed Matter,* M. D. Furnish, editor.

Hiltl, M., C. R. Hagelberg, R. P. Swift, T. C. Carney, and W. J. Nellis, 1999b, “ Dynamic response of Berea sandstone shock loaded under dry, wet, and waterpressurized conditions”. Proceedings, International Association for the Advancement of High Pressure Science and Technology (AIRAPT) International Conference on High Pressure Science and Technology (AIRAPT-17), July 25 - July 30, 1999, University of Hawaii, Honolulu, Hawaii, USA.

Isaaks, E. and R. Srivastava, 1989, *An Introduction to Applied Geostatistics*, Oxford University Press, New York.

Journel, A. and C. Huijbregts, 1978, *Mining Geostatistics*, Academic Press, London.

Lévesque, J. and D. J. King, 1999, “Airborne digital camera image semivariance for evaluation of forest structural damage at an acid mine site”, *Remote Sens. Environ.*, Vol. 22, pp. 211--227.

Matheron, G., 1963, “ Principles of geostatistics”, *Economic Geology,* Vol. 58, pp. 1246-1266.

McLeod, H. O., 1983, “The Effect of Perforating Conditions on Well Performance”, *J. Pet. Tech*., pp. 31-36.

Swift, R. P., C. R. Hagelberg, T. C. Carney, and D. Greening, 2000,

Table 1 - Experimental Conditions

Shot Number	Target Dim. (mm)	Flyer Material	Flyer Thickness (mm)	Impact Velocity (ms^{-1})	Impact Pressure (GPA)	Saturation Conditions
606	22.4x14.8	Al	6.25	760	6.1	Dry
611	22.4x14.5	Al	6.21	760	6.1	Wet
697	22.4x15.0	PMMA	6.12	450	1.4	Dry
700	22.4x14.8	Al	6.30	790	6.4	7.11 MPa
701	22.4x14.9	PMMA	6.14	440	1.3	7.65 MPa
739	22.4x14.9	PMMA	5.93	410	1.2	Wet

"Modeling Stress-Induced Damage from Impact Recovery Experiments", ASME/ETCE Joint Conference on Energy for the New Millenium (this volume).

Zhang, J., Wong, T.-F., Davis, D. M. (1990), "Micromechanics of Pressure-Induced Grain Crushing in Porous Rocks", *J. Geophys. Res.* Vol. 95, pp. 341-352.

Table 2 - Variogram Range Estimates

Shot #	Impact Conditions	Near Field Range (µm)	Far Field Range (µm)
606	6.1GPa dry	80	113
611	6.1GPa wet	95	107
700	6.4GPa pressurized	115	145
697	1.4GPa dry	114	145
739	1.2GPa wet	165	145
701	1.3GPa pressurized	134	146

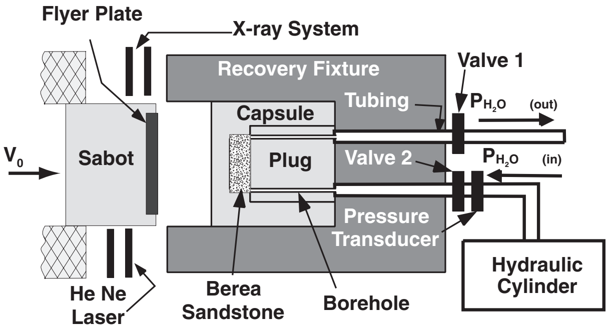

Figure 1. Schematic of experimental configuration (c.f. Hiltl et al, 1999). The sample is held in the aluminum capsule within the recovery fixture. The gas gun on the left launches the flyer plate into the fixture. Water pressurization is controlled through ports in the back of the recovery fixture.

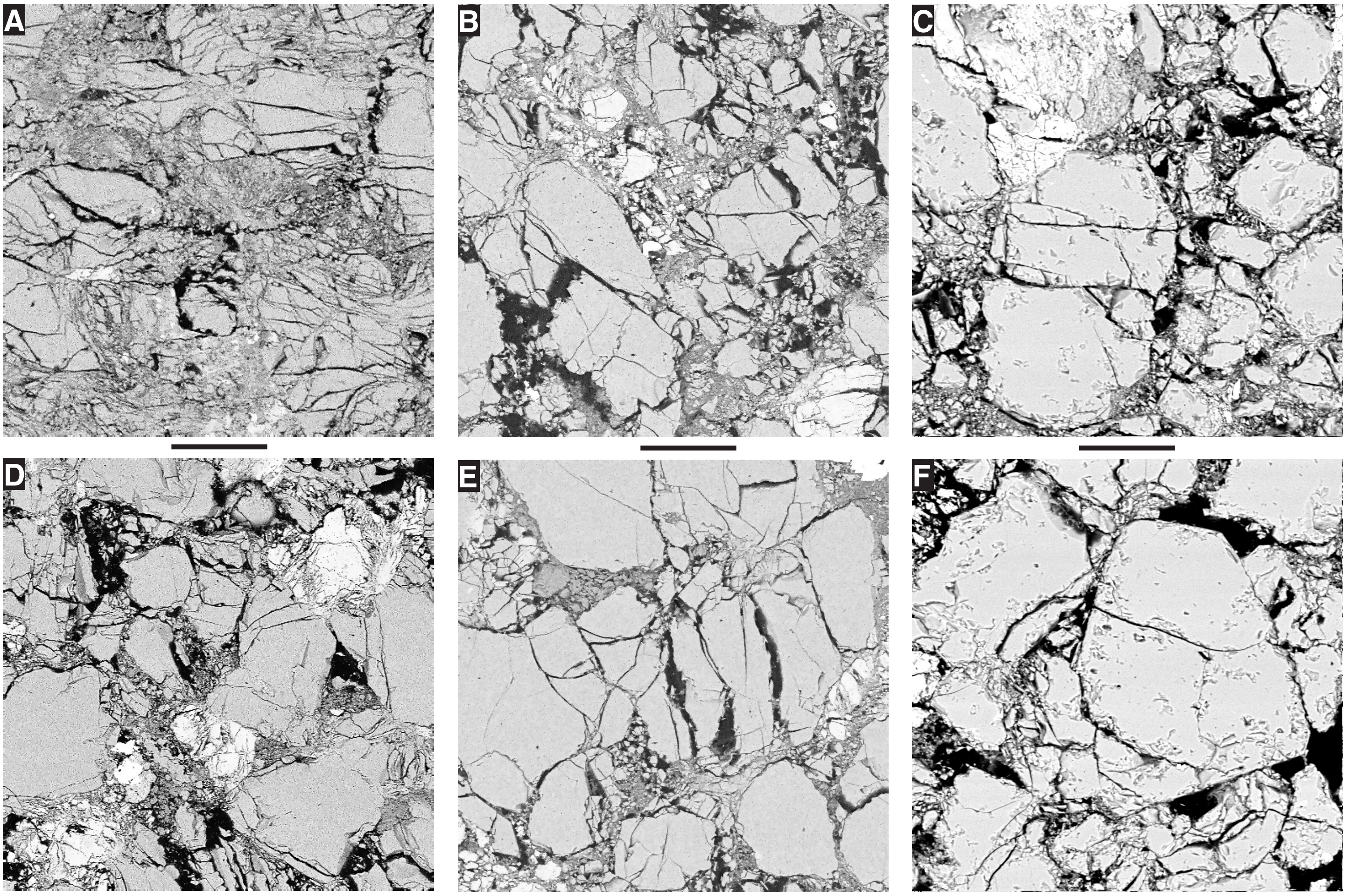

Figure 2. Examples of variations in damage from three different saturation conditions and two distances from the impact surface for impact pressures in the range 6.1 GPa to 6.4 GPa. The flyer plate struck the sample parallel to the top of each image. The top row of images are taken approximately 1mm from the impact surface (A,B,C) and the bottom row of images are taken approximately 12mm from the impact surface (D,E,F). The first column is from shot #606, a 6.1 GPa impact on dry Berea (A,D), the second column is from shot #611, a 6.1 GPa impact on water-saturated Berea (B,E), and the third column is from shot #700, a 6.4 GPa impact on Berea water-pressurized to 7.11 MPa (C,F).

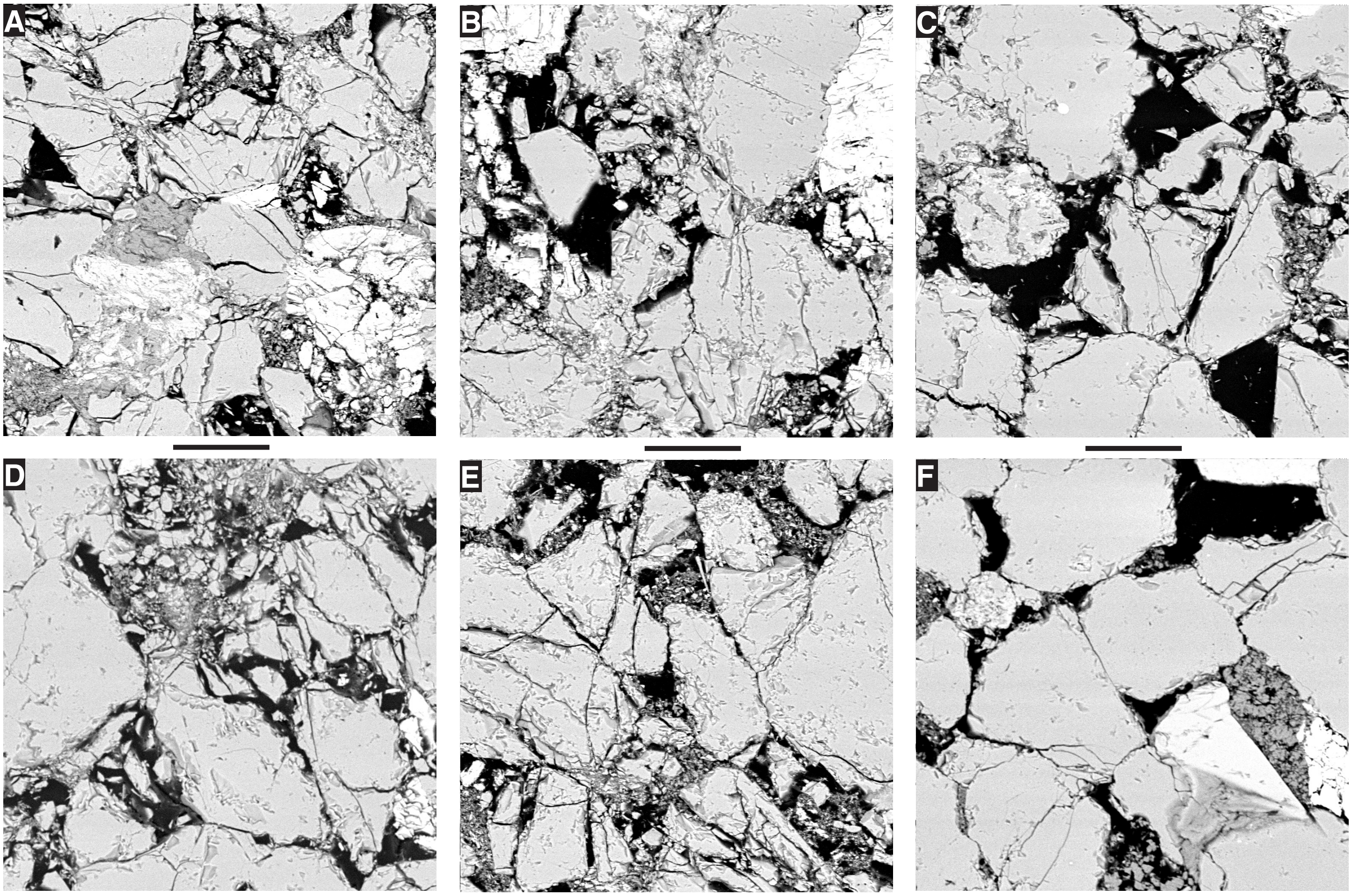

Figure 3. Examples of variations in damage from three different saturation conditions and two distances from the impact surface for impact pressures in the range 1.2 GPa to 1.4 GPa. The flyer plate struck the sample parallel to the top of each image. The top row of images are taken approximately 1mm from the impact surface (A,B,C) and the bottom row of images are taken approximately 12 mm from the impact surface (D,E,F). The first column is from shot #697, a 1.4 GPa impact on dry Berea (A,D), the second column is from shot #739, a 1.2 GPa impact on water-saturated Berea (B,E), and the third column is from shot #701, a 1.3 GPa impact on Berea water-pressurized to 7.65 MPa (C,F).

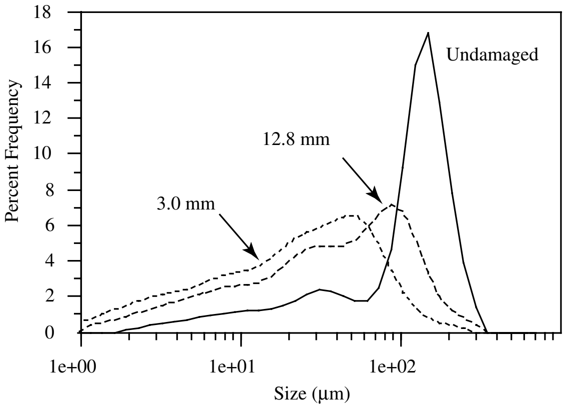

Figure 4. Laser particle size analyses for undamaged Berea (solid curve) and post-shock samples from a 6.1GPa dry experiment. Particle sizes were obtained from two portions of the shocked sample. One at a distance of 3 mm from the impact surface (dotted line) and one at a distance of 12.8 mm (dashed line). Note that only grains smaller than 150μm were included in the analysis by sieving the material.

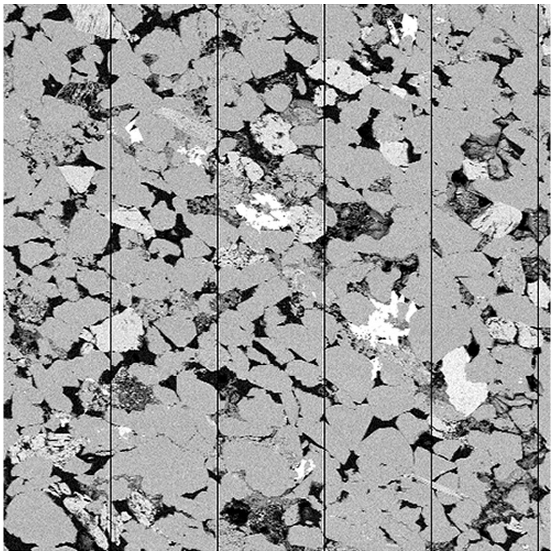

Figure 5. SEM of Berea sandstone at 100x magnification. The black vertical lines represent scan lines used in subsequent analyses and are spaced at 400μm intervals from the left.

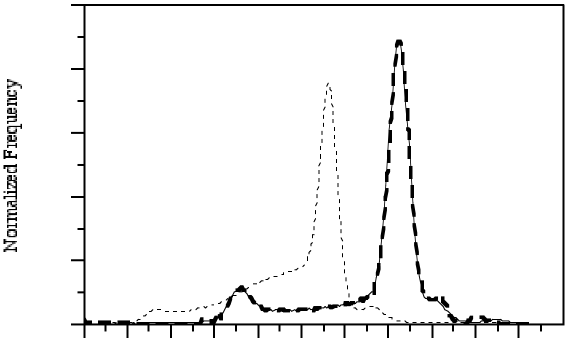

Figure 7. Histogram matching result showing the histogram to match (solid curve) the histogram to modify (dotted) and the result after modification (dashed curve).

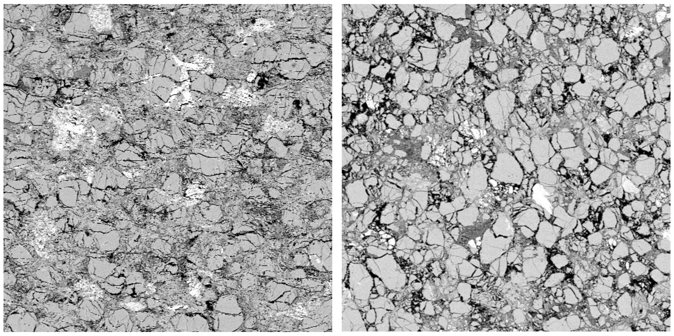

Figure 8. SEM images (100x) of 6.1 GPa shocked samples in the dry (A) and wet (B) states, used for statistical analysis.

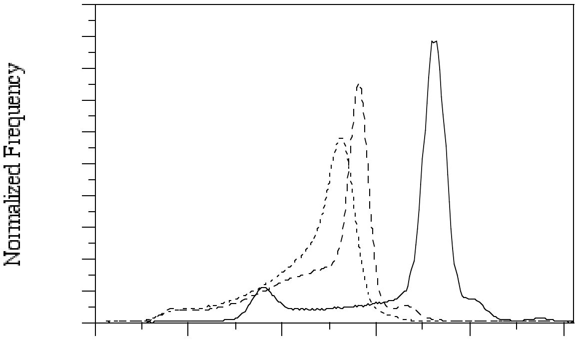

Figure 6. Histogram of SEM images of undamaged sandstone (solid) and post-shock samples (dotted and dashed). The variation in contrast is due to varying parameters on the SEM and must be considered as part of the experimental variability.

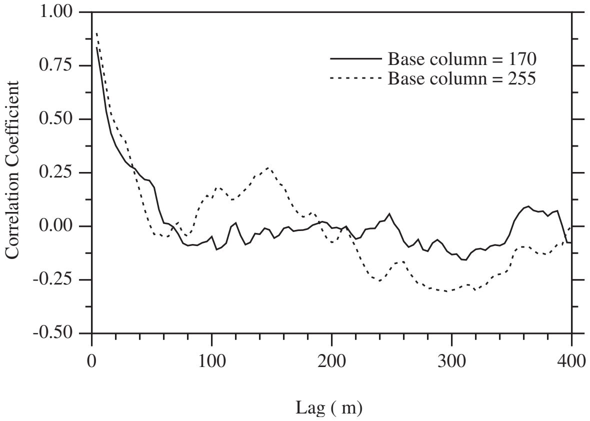

Figure 9. Correlation between image transects as a function of spacing between the transects for two different "base" locations in the image of undamaged Berea sandstone (Figure 4).

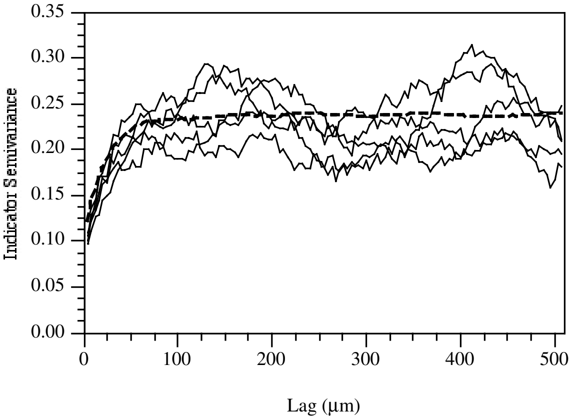

Figure 10. Indicator semivariograms of transects through undamaged Berea sandstone of Figure 4 (solid) and entire image (dotted).

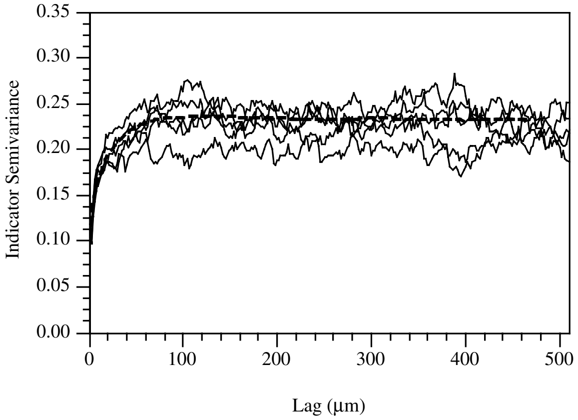

Figure 11a. Semivariograms of transects through 61kbar, dry sample, far field (shot #606).

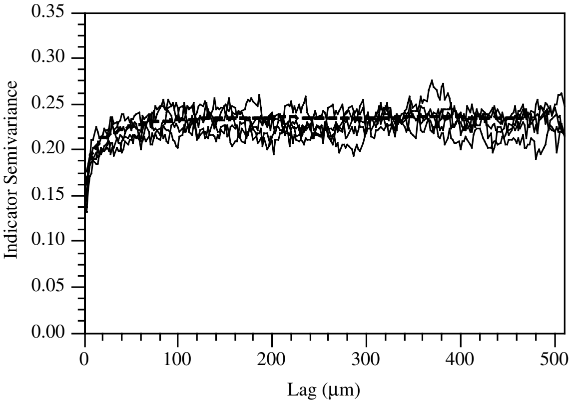

Figure 11b. Semivariograms of transects through 61kbar, dry sample, near field (shot #606).

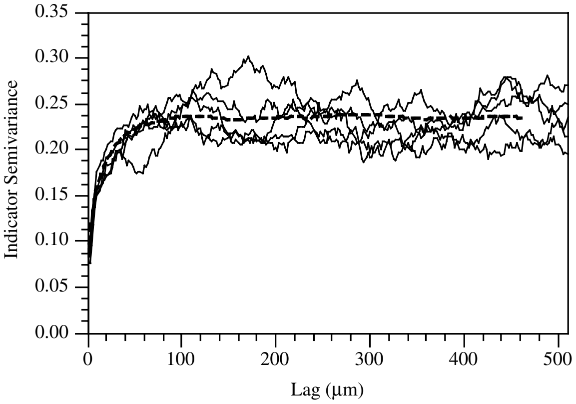

Figure 12a. Semivariograms of transects through 61kbar, wet sample, far field (shot #611).

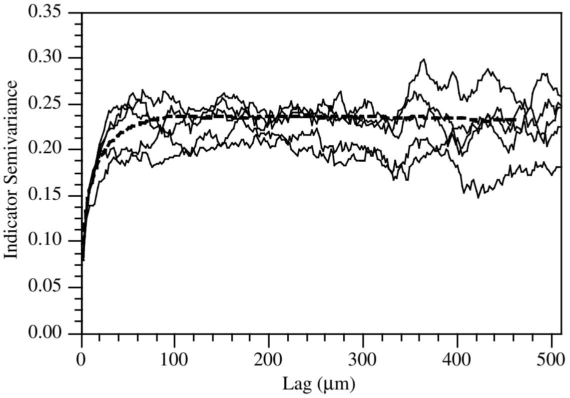

Figure 12b. Semivariograms of transects through 61kbar, wet sample, near field (shot #611).

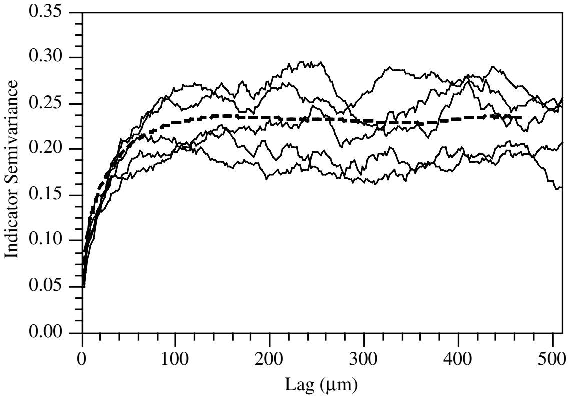

Figure 13a. Semivariograms of transects through 64kbar, pressurized sample, far field (shot #700).

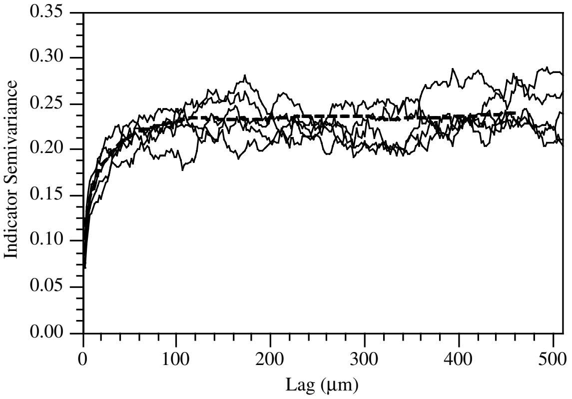

Figure 13b. Semivariograms of transects through 64kbar, pressurized sample, near field (shot #700).

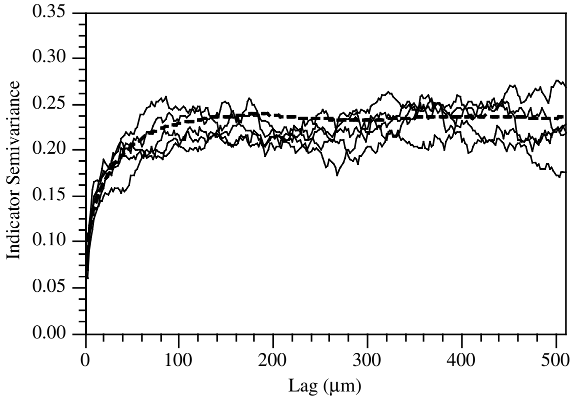

Figure 14a. Semivariograms of transects through 14kbar, dry sample, far field (shot #697).

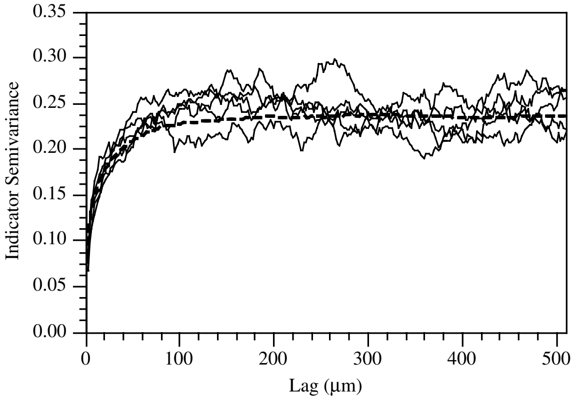

Figure 14b. Semivariograms of transects through 14kbar, dry sample, near field (shot #697).

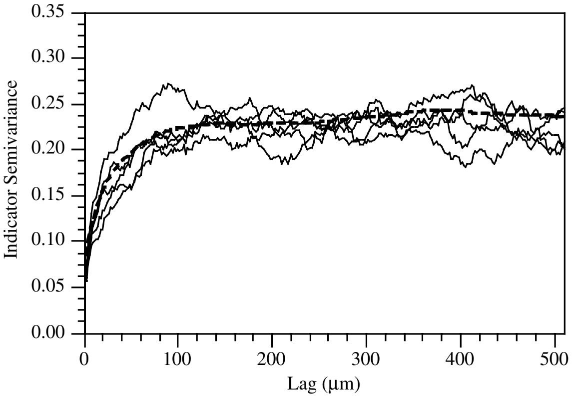

Figure 15a. Semivariograms of transects through 12kbar, pressurized sample, far field (shot #739).

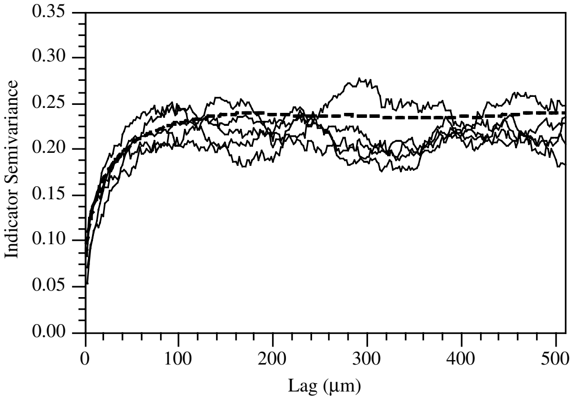

Figure 15b. Semivariograms of transects through 12kbar, pressurized sample, near field (shot #739).

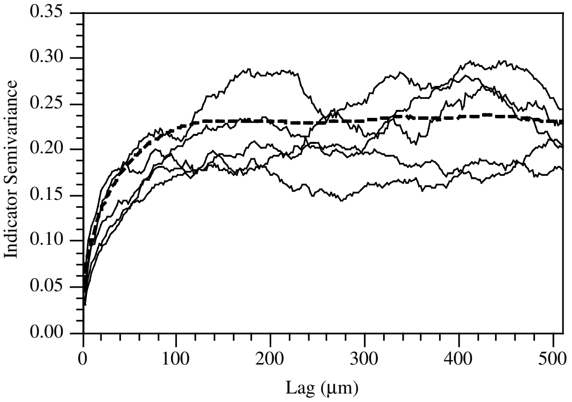

Figure 16a. Semivariograms of transects through 13kbar, pressurized sample, far field (shot #701).

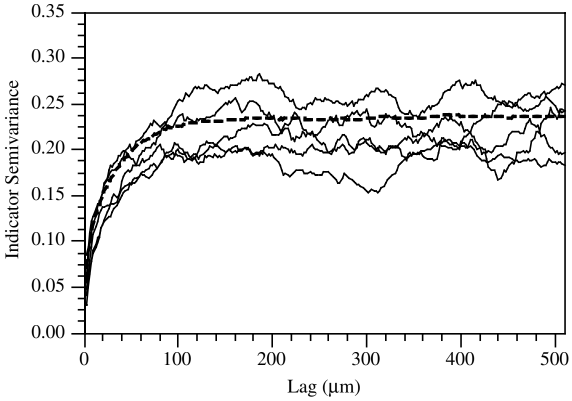

Figure 16b. Semivariograms of transects through 13kbar, pressurized sample, near field (shot #701).